Easy stabilization of Evonik Aeroxide P25 colloidal suspension by 4-Hydroxybenzoic acid functionalization

Julien G. Mahy [1,*], Sigrid Douven[2], Jonas Hollevoet[2], Nathalie Body[1], Tommy Haynes[1], Sophie Hermans[1], Stéphanie D. Lambert[2], Carlos A. Paez[2,†]

[1] *Institute of Condensed Matter and Nanosciences (IMCN), Université catholique de Louvain, Place Louis Pasteur 1, 1348, Louvain-la-Neuve, Belgium*

[2] *Department of Chemical Engineering – Nanomaterials, Catalysis & Electrochemistry, University of Liège, B6a, Quartier Agora, Allée du six Août 11, 4000 Liège, Belgium*

***Corresponding author:** Julien G. Mahy, Institute of Condensed Matter and Nanosciences (IMCN), Université catholique de Louvain, Place Louis Pasteur 1, 1348, Louvain-la-Neuve, Belgium. E-mail address: julien.mahy@uclouvain.be.

Keywords: Evonik Aeroxide P25, 4-hydroxybenzoic acid, grafting, colloid stability, photocatalysis.

Abstract

A new functionalization method was developed with the aim of producing stable TiO_2-based colloids starting from commercial Evonik Aeroxide P25 powder. The stability of P25 colloids was efficiently increased by grafting 4-hydroxybenzoic acid (4-HBA) on the P25 surface. Results highlighted that 4-HBA interacted with the surface of P25 through its carboxylic group. The key parameter for an optimized stability is the 4-HBA/P25 ratio. If the amount of 4-HBA is too high compared to the TiO_2 available surface, 4-HBA molecules preferentially interact with each other, therefore reducing their adsorption on P25.

Eight different amounts of 4-HBA were grafted on P25, producing stable colloids in both ethanol and water medium. In both media, the optimal properties and highest stability were obtained for a 4-HBA/TiO_2 mass ratio equal to 0.333.

This optimal sample was further tested and compared to pure P25 (used as reference material) for *p*-nitrophenol (PNP) degradation under UV-visible light without any stirring to highlight the beneficial effect of the powder stability. The photocatalytic results showed that the grafted sample reached a degradation up to 8 times higher than pure P25. This functionalization method is easy to implement and stabilizes colloids starting from any pre-synthesized powder. This versatility widens the field of applications, and opens the door for further developments in areas such as coatings.

Graphical abstract

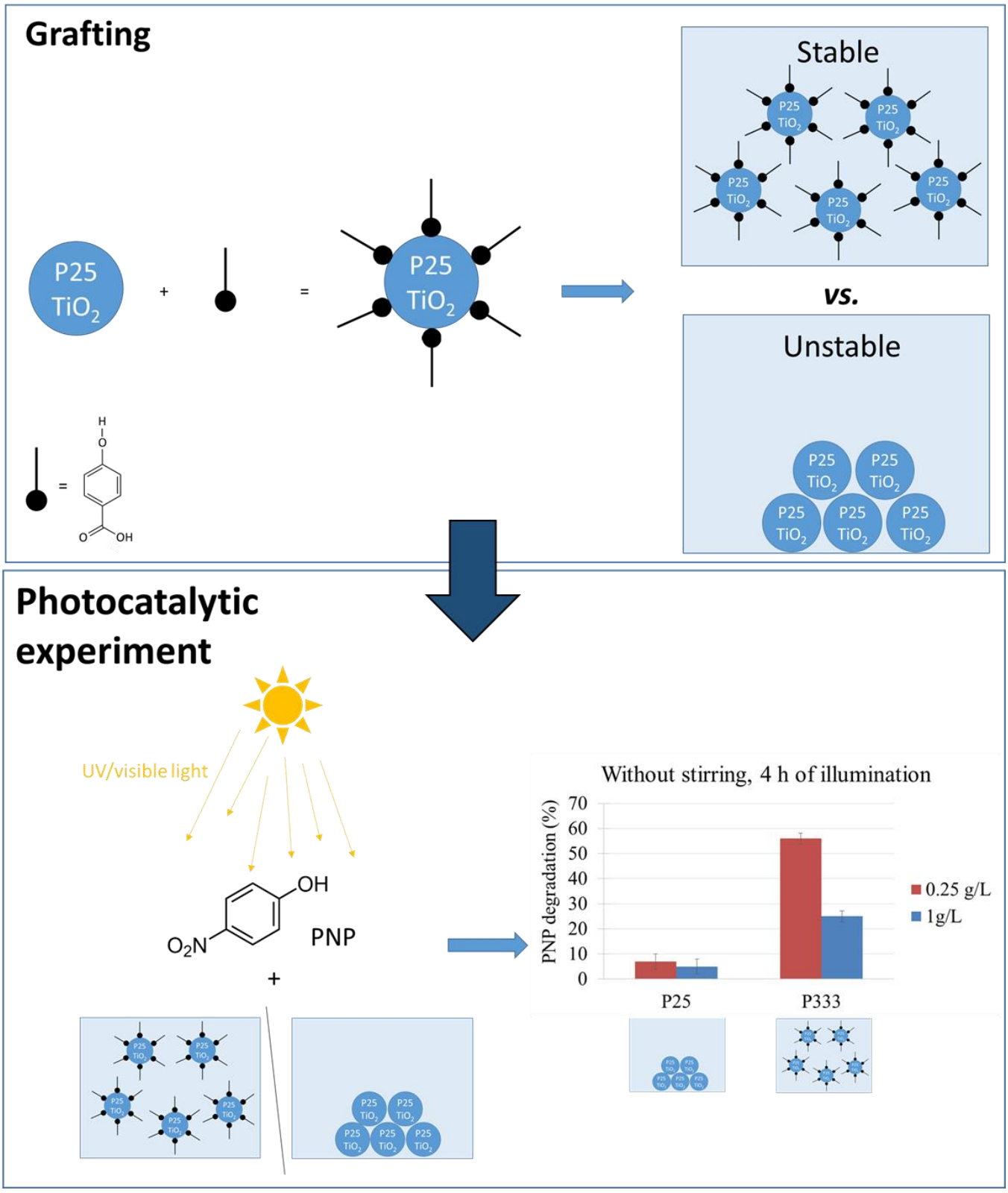
Grafting
P25 TiO2
+
=
P25 TiO2
Stable
P25 TiO2
vs.
Unstable
P25 TiO2
Photocatalytic experiment
UV/visible light
OH
O2N
PNP
+
Without stirring, 4 h of illumination
PNP degradation (%)
70
60
50
40
30
20
10
0
0.25 g/L
1g/L
P25
P333

1. Introduction

Nowadays, nanoparticles are present in a large range of applications due to their unique size-dependent properties such as electrical, magnetic, mechanical, optical, and chemical characteristics, which largely differ from those in the bulk [1,2]. According to their applications, different shapes and organization of nanoparticles are produced, such as nano-powder, aggregates, thin layers or nano-colloids.

Nano-TiO_2 colloids offer interesting photocatalytic and easy-to-clean properties. For nano-colloids, the stability in liquid suspensions is crucial to ensure a reproducible behavior whatever the application. Indeed, starting from nano-colloids, thin nano-coatings can be produced by different techniques such as dip-coating [3–5], spray-coating [6], spin-coating [7] or electrophoretic deposition [8]. Dip-coating [3,4] requires high stability of the colloid to produce several layers on the substrate. In fact, once the process parameters are optimized (up-speed, down-speed of the substrate...), the properties (such as the thickness and roughness) of successive layers should be maintained if precipitation is avoided. For spray-coating [6], if precipitation occurs, it can block the nozzle and lead to non-reproducible coatings. In electrophoretic deposition [8], the film is produced on an electrode thanks to the electrophoretic motion of charged particles in the colloid suspension caused by the applied electrical field. Stable suspensions with well-dispersed charged particles are therefore required [8].

Nano-colloids can also be used as catalysts in continuous-flow microreactors to conduct a large range of reactions. In photochemistry [9] for example, radical species are produced using nano-TiO_2 colloids to degrade pollutants or to produce high added-value products. The advantages of microreactors, especially in photochemistry, are an improved light penetration, an accurate control of irradiation time, an efficient mass and heat transfer, a safe and efficient handling of transient species [9,10]. Nevertheless, the nano-colloids need to be stable in order to avoid the clogging of the microchannels [9].

Several techniques are described to achieve colloidal stability. A first solution is to increase the particle charge. Indeed, charged nanoparticles repulse each other, leading to a better stability [11]. The adsorption of metal ions at the surface of the nanoparticles increases their charges [11]. This adsorption can be done thanks to the addition of a salt in the suspension. However, a too high ionic strength of the suspension can result in a lower particle stability and subsequent precipitation. A second approach to increase the stability is the use of a dispersant [12–18]. The dispersant can (i) charge the surface of the particles, or (ii) act as steric dispersant by anchoring long-chain molecules at the nanoparticle surface [12–16]. Nevertheless, the long-chain molecules often introduce an organic contamination in the sample that needs to be eliminated after deposition, by calcination for example. The adhesion of the dispersant to the nanoparticle surface is also a critical point. Indeed, a strong interfacial adhesion is necessary to keep the stability of the suspension [8].

Increasing the adhesion between the dispersant and the nanoparticles is a topic of interest. An innovative bio-mimetic method, inspired by the mussel adhesion in water environment, has been studied in recent years [8]. This method is based on the grafting of catechol or salicylate-like molecules at the surface of the nanoparticles to increase their colloidal dispersion [19–22]. These molecules show a great adhesion to metal oxides such as TiO_2, ZnO or Al_2O_3 [19]. Several mechanisms have been proposed depending on the type of catechol-like molecule and on the metal oxide substrate [19–22]. This method seems to be a promising way to produce stable metal oxide suspensions [19–22].

Moreover, the adsorption of complexants [23,24] at the surface of TiO_2 can enhance the rate of electron transfer from the conduction band of the dioxide to electron acceptor molecules in solution [23,24]. This phenomenon allows to increase the recombination time between the photo-generated electrons and holes and leads to a more efficient formation of active species to conduct photocatalytic reactions for example.

In this work, stable TiO_2-based colloids were produced by grafting, in solution, 4-hydroxybenzoic acid (4-HBA) at the surface of commercial Evonik Aeroxide P25 powders. The optimal amount of 4-HBA grafted at the P25 surface was determined according to the stability of the produced colloids. The grafting mode was studied thanks to Thermogravimetric-Differential Scanning Calorimetry (TG-DSC) and Fourier Transform Infrared (FT-IR) analyses.

To objectify the impact of the grafting, photocatalytic experiments were carried out. The photocatalytic activity was assessed through the degradation of a model pollutant, *p*-nitrophenol (PNP), without and with stirring. The enhancement of the performance was estimated for the optimized sample of grafted P25 in comparison to pure P25.

2. Materials and Methods

2.1.Evonik Aeroxide P25 powder functionalization

For the powder functionalization, Evonik Aeroxide P25 powder and 4-hydroxybenzoic acid (4-HBA, Aldrich Reagent Plus®) were used as reagents and used as received. First, a saturated aqueous solution of 4-hydroxybenzoic acid is prepared, at a concentration of 5 g/L. Then a defined mass of Evonik Aeroxide P25 powder is added to 1 L of saturated solution, the different amounts being used are given in Table 1. The mixture is stirred for 16 h, protected from the ambient light by aluminum foil. Then, the liquid is centrifuged at 7000 rpm until most of the solid is at the bottom of the test tube. The supernatant composed of 4-hydroxybenzoic acid and a small amount of P25 is eliminated. The residual solid is redispersed in water with ultrasonic bath before centrifugation at 7000 rpm and removal of the water. The residual solid is dried at 90 °C and finally grinded to obtain a yellow powder. A total of 8 different functionalized powders are produced. The pure Evonik Aeroxide P25 powder is also used as reference leading to 9 samples. The different names of the powders are defined in Table 1.

Table 1: Amount of TiO_2 and 4-hydroxybenzoic acid in the samples

Powder Name	TiO_2 concentration in 4-HBA solution (g/L)	4-HBA/TiO_2 ($g_{4\text{-HBA}}/g_{TiO2}$)
P25	-	-
P5000	1	5
P1667	3	1.667
P833	6	0.833
P556	9	0.556
P417	12	0.417
P333	15	0.333
P167	30	0.167
P83	60	0.083

2.2.Colloid formation from functionalized Evonik Aeroxide P25 powder

Two solvents are used for the preparation of the colloidal suspensions: absolute ethanol (Merck, > 99 %) and deionized water. The powder is placed in 10 mL of the solvent in an ultrasonic bath for 2 h. The amounts of powder are calculated in order to reach 0.25 g/L, 0.5 g/L, 1 g/L, 3 g/L, 5 g/L for each solvent and each functionalized powder, leading to 90 different colloids. The colloids are labelled by E (ethanol) or W (water), followed by the powder name (see Table 1), and finally the powder concentration. As an example, W-P333/5 corresponds to the colloid of powder P333 in water at the concentration of 5 g/L.

2.3.Characterizations

The weight loss of the powders is determined by Thermogravimetric-Differential Scanning Calorimetry (TG-DSC) up to 800 °C. This weight loss is related to the amount of 4-hydroxybenzoic acid grafted onto the Evonik Aeroxide P25 powder. The weight loss at the different temperatures is used to identify some compounds. The measurements are performed with a Sensys evo device from Setaram Instrumentation.

Fourier transform infrared (FT-IR) spectra in the region of 400–4000 cm^{-1} are recorded at room temperature with a Spectrum One FT-IR Spectrometer from PerkinElmer. All catalyst powders are dispersed in KBr (1 wt% for all samples) before analysis.

The stability of the colloids is evaluated by observing the 10 mL colloids in test tubes after 3 days at rest. After these 3 days, 1.5 mL of supernatant liquid are sampled and dried in an oven to estimate the residual powder concentration in suspension.

In the colloids, the sizes of TiO_2 aggregates are estimated by dynamic light scattering (DLS) in a DelsaNano C device from Beckman Coulter. This measurement gives a hydrodynamic diameter of aggregates [25]. The zeta potential is measured on the water colloids with a DelsaNano C device from Beckman Coulter, giving information about colloid stability.

Transmission electron microscopy is performed on a LEO 922 OMEGA Energy Filter Transmission Electron Microscope operating at 120 kV. For sample preparation, few milligrams of each sample are dispersed in ethanol using sonication. Then, a few drops are deposited on a copper grid (CF-1.2/1.3-2 Cu-50, C-flat™, Protochips, USA) and dried at ambient temperature for the night before measurement.

DRUV-Vis analyses are performed on a UV 3600 Plus UV-VIS-NIR spectrophotometer from Shimadzu. Measurements are performed in diffuse reflectance mode. The spectra range of analysis is from 200 to 600 nm. The baseline is performed using spectralon as a reference. The spectra are transformed using the Kubelka-Munk function [26,27] to produce a signal, normalized for comparison between samples, enabling to calculate the band gaps ($E_{g,direct}$). The details of this treatment method are widely described elsewhere [28,29].

XPS analyses are performed with a SI-X-probe 100/206 spectrometer (Surface Science Instruments), equipped with a flood gun (8 eV) for surface charge neutralization. A few milligrams of each sample are deposited on a double-sided adhesive support clung onto a brass

cup, and then introduced into a Macor® carousel topped by a nickel grid in order to avoid charge effects. The analyses are then performed, without further sample preparation at room temperature with an analysis chamber pressure of 10^{-6} Pa.

The main peaks analyzed in the different samples are C *1s*, N *1s*, O *1s*, and Ti *2p*. Data treatment is executed with the CasaXPS software (Casa Software Ltd, Japan) using a Gaussian/ Lorentzian (85/15) decomposition treatment and a Shirley-type baseline subtraction. All XPS spectra are calibrated using the C-(C,H) component of the C *1s* peak localized at 284.8 eV.

2.4.Photocatalytic activity

The photocatalytic activity of the best sample in the form of powder is assessed by measuring the degradation of *p*-nitrophenol (PNP) after 4 h, in triplicate and in water. The degradation percentage of PNP, D_{PNPi}, is given by Eq. 1 [30]:

$$D_{\mathrm{PNP}i}(\%) = \left(1 - \frac{[\mathrm{PNP}]_i}{[\mathrm{PNP}]_0}\right) * 100\% \quad (1)$$

where $[\mathrm{PNP}]_i$ represents the residual concentration of PNP at time t = i h and $[\mathrm{PNP}]_0$ represents the initial concentration of PNP at time t = 0 h.

The photocatalytic activity of the samples is estimated under halogen light (UV/visible light) [30]. The experimental setup is shown in [30,31]. The experiments follow the procedure described in [30,32]. The concentration of PNP is estimated by UV/Vis spectroscopy (GENESYS 10S UV–Vis from Thermo Scientific) at 318 nm. The volume of each flask is 10 mL. For each catalyst, three flasks are exposed to light to calculate the PNP degradation and one is kept in the dark (dark test) to evaluate PNP adsorption on the samples [30,32]. Additionally, a flask containing only PNP without any catalyst is exposed to the light for 24 h (blank test). This blank test shows that there is no decomposition of PNP under halogen

illumination. In each flask, the initial concentration of PNP is 10^{-4} M [30,32], the initial pH is 4 and the catalyst concentration is 0.25 or 1 g L^{-1}. Experiments are conducted in test tubes fitted with a sealing cap. These tubes are placed in a cylindrical glass reactor with the halogen lamp in the center. The halogen lamp has a continuous spectrum from 300 nm to 800 nm (300 W, 220 V), measured with a Mini-Spectrometer TM-UV/vis C10082MD from Hamamatsu [30,32]. The reactor and the lamp are maintained at constant temperature (20 °C) by a water cooling system [30,32]. Aluminum foil is used to cover the outer wall of the reactor to prevent any interactions with the room lighting. The PNP degradation due to photocatalysis is equal to the total PNP degradation minus the PNP adsorption estimated with the dark test [30,32]. The photocatalytic activity is evaluated without stirring to highlight the dispersion capacity of the prepared materials. Photocatalytic experiments are also carried out with stirring to highlight the beneficial effect of the stability brought by the 4-HB grafting by comparison with experiments without stirring.

2.5.Recycling experiments

In order to assess the stability of the 4-HBA grafting, recycling photocatalytic experiments are performed. After the initial photocatalytic experiment as described in Section 2.4 (for a catalyst concentration of 0.25 g/L and without stirring), the solid sample is recovered by washing and centrifugation (10000 rpm for 15 min) followed by drying at 120 °C overnight. Five recycling cycles are applied to the re-used photocatalysts, with washing and drying steps between each photocatalytic experiment. So, the P333 and P25 samples are used for six successive photocatalytic experiments, for a total of 24 h of illumination. A mean PNP degradation rate on the six experiments is calculated.

3. Results and Discussion

3.1.Functionalization of Evonik Aeroxide P25 TiO_2 powder with 4-HBA: TG-DSC analysis

The weight percentage of 4-HBA grafted on TiO_2 is presented in Figure 1 and is calculated from the weight loss measured by thermogravimetry for all samples as defined in Table 1. Figure 1 shows that the amount of 4-HBA grafted per gram of TiO_2 reaches a peak before decreasing. This peak corresponds to the maximum functionalization rate of the TiO_2 particles. The optimal grafted powder is P556.

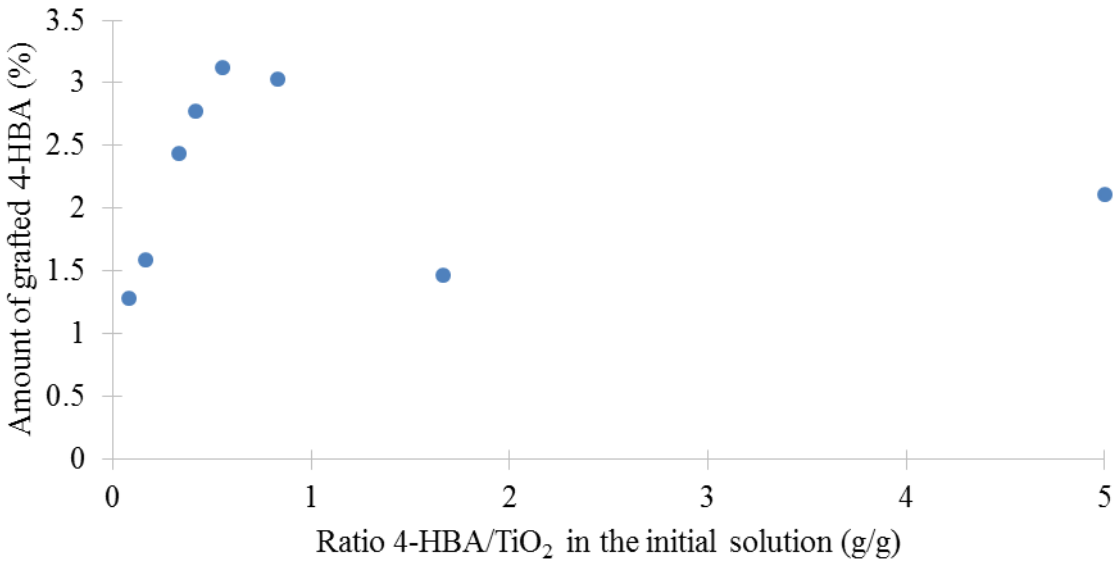

Figure 1: Amount (%) of 4-HBA grafted on TiO_2 for all samples, calculated from thermogravimetric results.

Thermogravimetric data are also used to determine the way 4-HBA molecules are grafted on TiO_2 powder. The solute concentration at equilibrium in the substrate (= the concentration of 4-HBA in the functionalized TiO_2 powder) is plotted as a function of the concentration of solute at equilibrium (= concentration of 4-HBA in the liquid eliminated after the first centrifugation). The shape of this curve, called adsorption isotherm, is analyzed according to Giles *et al.* [33]. The solute concentration at equilibrium in the substrate [mol 4-HBA/g of TiO_2] is calculated using the mass of 4-HBA grafted per gram of TiO_2 (thermogravimetric data from Figure 1) and the molar mass of 4-HBA ($MM_{4\text{-HBA}}$ = 138.12 g/mol). The equilibrium solute concentration [mol 4-HBA/L] is obtained by subtracting the amount of 4-HBA grafted on TiO_2 powder from

the initial concentration of 4-HBA (5 g/L) in the functionalization solution. These results are presented in Figure 2.

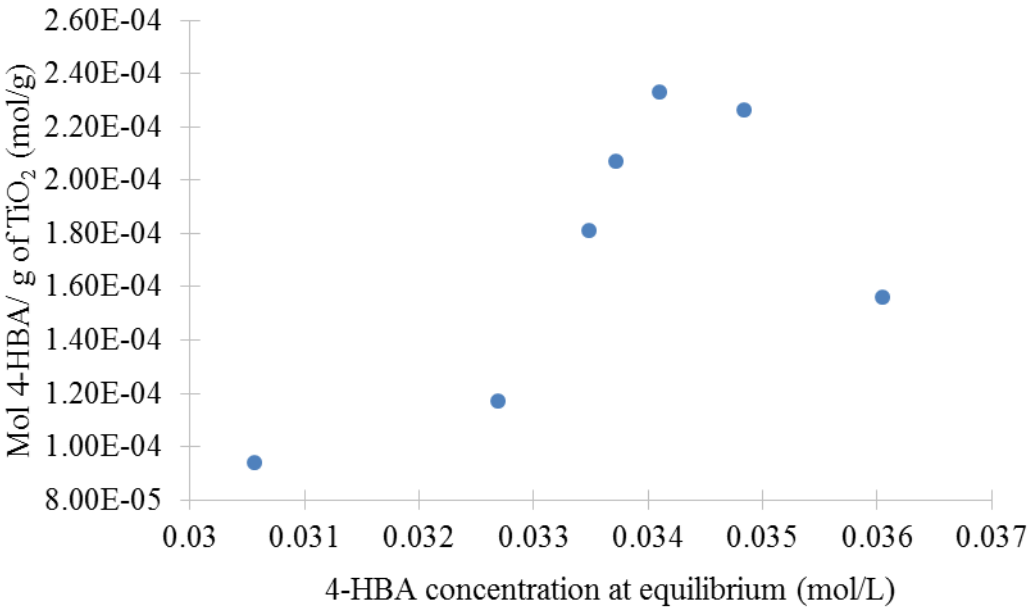

Figure 2: Adsorption isotherm of 4-HBA on TiO_2 particles.

In the work of Giles *et al.* [33,34], the classification of adsorption isotherms for solutes in dilute solution is studied. Four main classes of adsorption isotherms are detailed depending on the adsorption mechanism [33,34]. The comparison of Figure 2 with the reference Figures of Giles *et al.* [33,34] allows to determine that the obtained isotherm is of S-type [33,34]. The S isotherms are observed in the case of a cooperative adsorption in which the solute is adsorbed in a row or cluster arrangement. In the case of a monofunctional solute, *i.e.* not containing two functions of the same type, this functional group will adsorb in a so-called "high" position as shown in Figure 3 a. In this configuration, the solute is fixed to the surface at one end and may be perpendicular to the surface or slightly inclined. On the contrary, if the solute possesses two identical functional groups, *i.e.* bifunctional, it will tend to adsorb parallel to the surface ("low"

position) as in Figure 3 b. In our study, 4-HBA is a monofunctional solute, therefore favoring the high position.

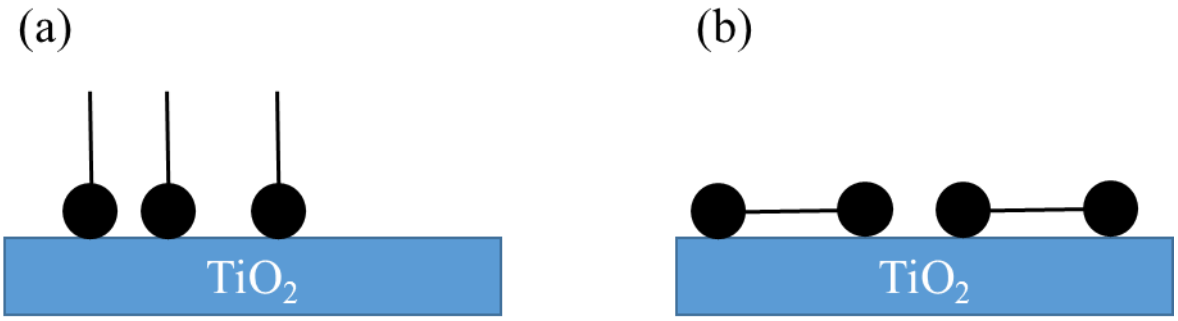

Figure 3: (a) high position adsorption and (b) low position adsorption [33]**.**

The shape of the adsorption isotherm is rather particular because beyond the equilibrium solute concentration of 0.03417 mol/L, which corresponds to a mass ratio 4-HBA/TiO_2 of 0.556 g/g, the amount of adsorbed solute decreases. This maximum is, according to another work of Giles *et al*. [35], probably due to an increase in associative interactions within the solution i.e. between 4-HBA molecules. These interactions are favored to the detriment of the interactions between TiO_2 and 4-HBA, which leads to a decrease in the rate of functionalization.

Thermogravimetric analyses tend to prove that 4-HBA molecules are preferentially grafted perpendicularly to the surface of TiO_2 particles. Anyway, at a limit, the maximum area occupied by a molecule of 4-HBA corresponds to the area of a circle whose diameter is equal to the greatest distance separating two ends of the molecule as shown in Figure 4. Therefore, the maximum percentage of TiO_2 surface covered by a monolayer of perpendicular 4-HBA molecules can be estimated.

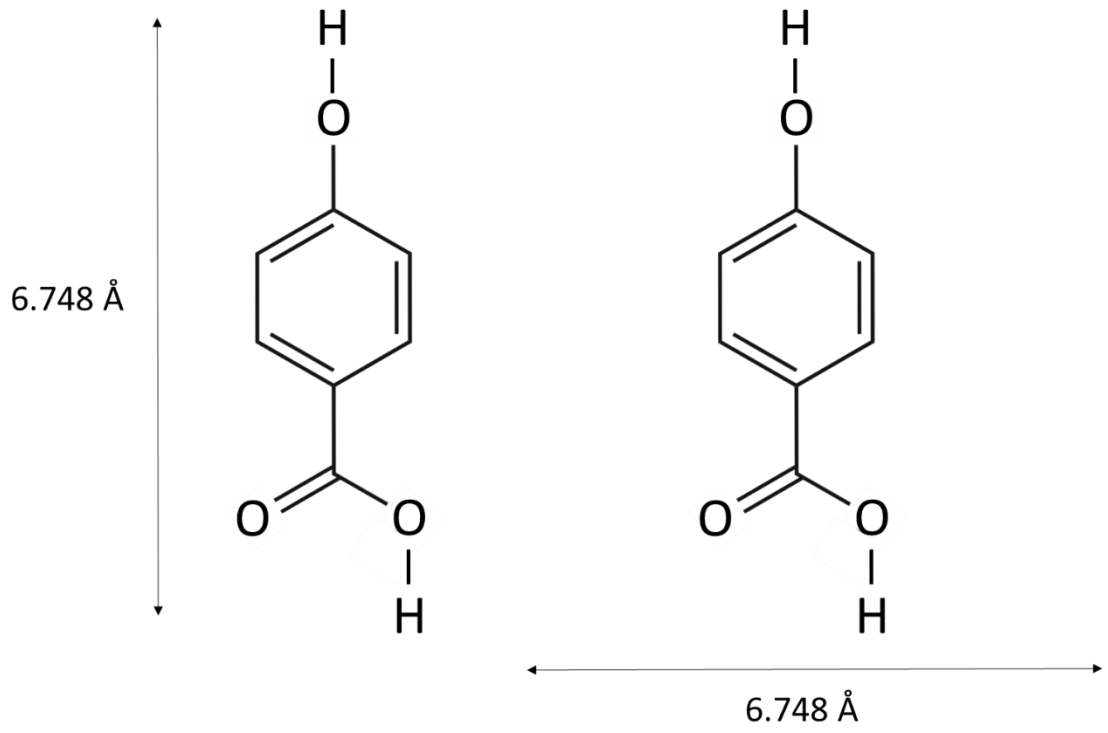

Figure 4: Illustration of the maximum surface occupied by a 4-HBA molecule grafted perpendicularly to a TiO_2 particle surface.

This distance is 6.748 Å for a 4-HBA molecule (ChemSketch). The corresponding area is therefore $\pi*6.748^2/4$ Å^2. Furthermore, as the specific surface of the Evonik Aeroxide P25 TiO_2 powder is around 50 m^2/g [36], the fraction of the surface of TiO_2 particles coated by a monolayer of vertical 4-HBA molecules can be estimated. Results are reported in Table 2. The detail of the calculations is given in Supplementary Materials.

Table 2: Percentage of the TiO_2 surface covered by 4-HBA in the samples

Powder Name	4-HBA/TiO_2 ($g_{4\text{-HBA}}/g_{TiO2}$)	Percentage of covered surface (%)
P25	-	0
P5000	5	65.8
P1667	1.667	45.7
P833	0.833	94.5
P556	0.556	97.1
P417	0.417	86.8
P333	0.333	76.2
P167	0.167	49.7

P83	0.083	40.01

These values (Table 2) indicate that, in the case of P556 powder, almost the entire surface of titanium dioxide particles would be coated with vertical 4-HBA molecules. The results of the surface covering are in good agreement with the adsorption isotherm. Indeed, for a 4-HBA/TiO_2 mass ratio equal to 0.56 g/g, the surface of the TiO_2 particles seems completely covered with 4-HBA. So there is no free space for other molecules to be adsorbed on the surface which will promote interactions between 4-HBA molecules within the solution, causing a decrease in adsorption of the solute on the TiO_2 particles. Adsorption of 4-HBA molecules on TiO_2 is therefore limited by the surface available for their grafting on the particles.

TG-DSC measurements were also performed on all the powders. All measurements follow the same trends. As an example, curves for P333 sample are presented in Figure 5.

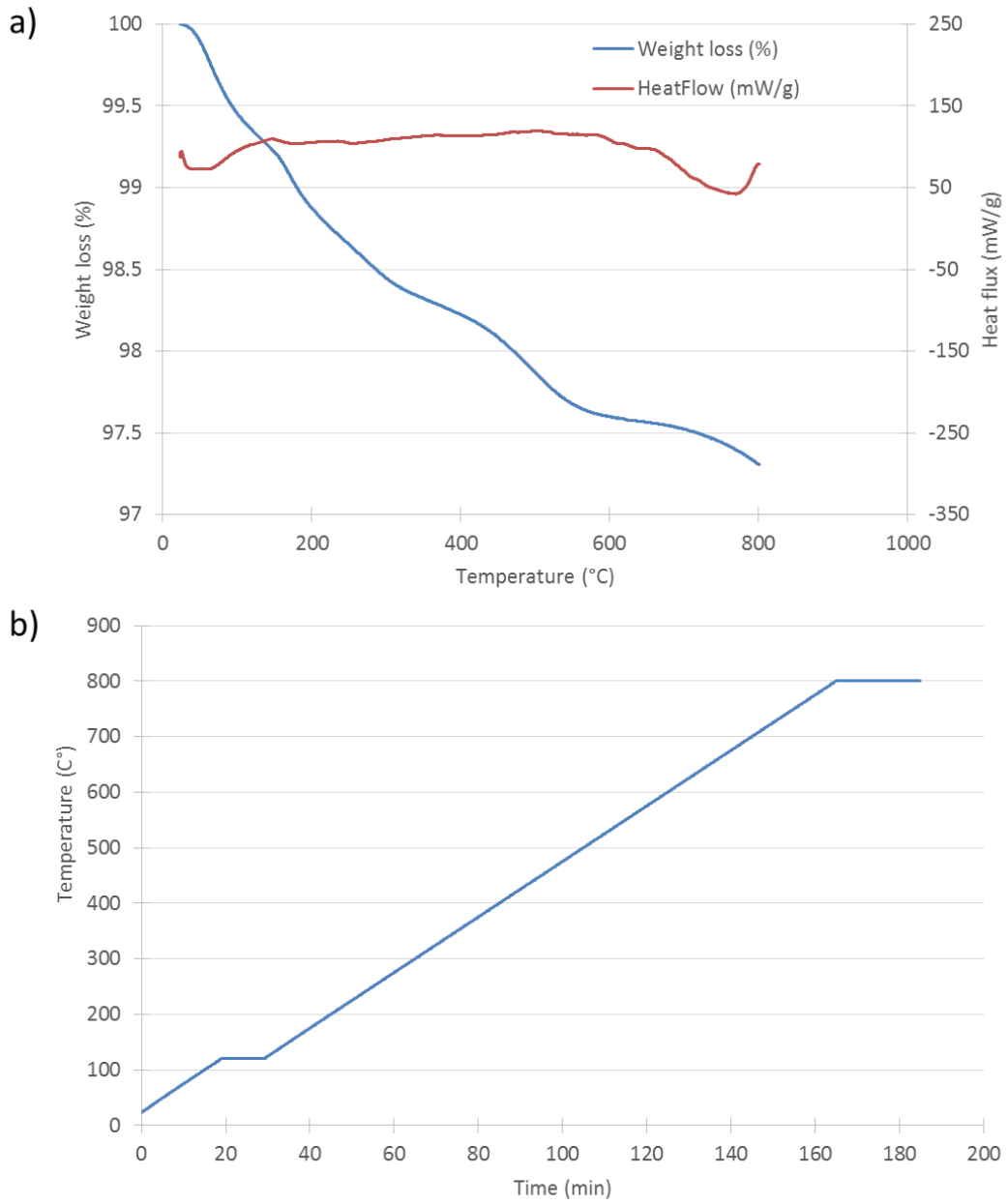

Figure 5: (a) TG-DSC measurement for P333 sample and (b) the corresponding temperature ramp.

On the basis of the typical TG experiment curves of Wirth *et al.* [37], some trends can be detected. First, the convexity of the heat flux curve (Figure 5) between 40 °C and 90 °C is similar to the one observed in type 2 curve of Wirth *et al.* [37]. This indicates a rapid loss of mass often due to dehydration or evaporation. The second part of the curve is representative of a decomposition in several stages, rather similar to type 4 in [37].

The differential thermogravimetry analyses of functionalized powders were calculated and are also very similar between samples. The chart for the P333 powder is represented as example in Figure 6.

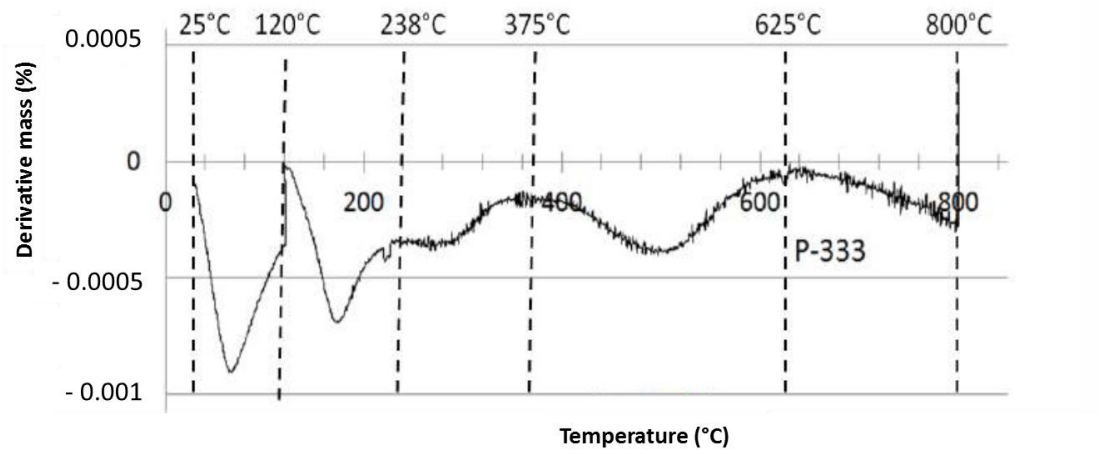

Figure 6: Differential thermogravimetry of P333 sample.

In Figure 6, four peaks are identified in the following temperature ranges: 25 - 120 °C, 120 - 238 °C, 238 - 375 °C and 375 - 625 °C. The first peak, in the range 25 °C to 120 °C and whose maximum mass loss rate is around 100 °C, corresponds to the dehydration of the powders. The position of this peak is similar to the results of the work carried out by Nazeeruddin *et al.* [38] and Amirnasr *et al.* [39]. Furthermore, a heat flux, is observed in the DSC curves (Figure 5) at around 120 °C. This is consistent with dehydration, known to be an endothermic process. All details of the calculations are presented in the Supplementary Materials (Section 2, Figure S1 and Tables S2-S3).

The second peak, ranging from 120 °C to 238 °C, probably corresponds to the elimination of hydroxyl groups of 4-HBA molecules grafted on the TiO_2. In this temperature range, the powders lose around 12.2 % of their mass. Assuming that, above 120 °C, the loss of mass is exclusively due to the degradation of 4-HBA, the experimental 12.2 % value is close to the theoretical mass content of OH groups (12.4 %) in the 4-HBA. This observation is consistent with the results of infrared spectroscopy that indicate that the 4-HBA is fixed to the surface of

TiO_2 particles by its carboxyl groups (see Section 3.2 and Figure S1 for Scheme of grafted molecule). This strengthens the idea that the hydroxyl groups will be the first to be eliminated after a change in temperature.

In the same way as above, by grouping the two peaks in the temperature range 238 -625 °C, an average dry weight loss of 56.3 % is calculated. This can probably be attributed to the elimination of the benzene ring of 4-HBA which represents 55.4 % of its mass.

Finally, above 625 °C, the average weight loss of 31.5 % is due to elimination of the CO_2 group, which is 32.1 % of the mass of the acid. The removal of CO_2 in this temperature range is likely since, in the case of $CaCO_3$, carbon dioxide is removed in temperatures ranging from 600 °C to 762 - 850 °C [40,41]. It confirms that the 4-HBA molecule is grafted by its carboxyl groups to the surface of the TiO_2.

3.2. Functionalization of Evonik Aeroxide P25 TiO_2 powder with 4-HBA: FTIR analysis

The infrared spectrum of TiO_2 P25 is shown in Figure 7 and Figure S2. The absorption bands of this spectrum are identified according to Wu *et al.* [8]. Thus, the band at 3392 cm^{-1} corresponds to stretching vibrations of OH groups in water molecules absorbed on the surface of TiO_2 and OH surface groups of titania. The peak at 1639 cm^{-1} is attributed to angular deformations of surface OH groups. Finally, the broad absorption band below 800 cm^{-1} is connected to characteristic Ti-O absorptions of TiO_2. As expected, the P25 powder alone is composed of TiO_2 with surface hydroxyl groups and surface absorbed water.

The absorption spectrum of 4-HBA is shown in Figure 8 (and Figure S3) and can also be analyzed based on Wu *et al.* [8]. The absorption band at 3353 cm^{-1} is characteristic of the -OH group of the 4-HBA molecule and possibly to the presence of water in the powder. The peaks at 1672 cm^{-1} and 1591 cm^{-1} are due to the elongation of C = O groups and the vibration of the

C - C bonds of the aromatic ring respectively. The two peaks at 1508 cm^{-1} and 1416 cm^{-1} are the asymmetric and symmetric stretching of carboxyl groups. The absorption band at 1165 cm^{-1} is due to the angular deformation (bending) of alcohol C - OH groups. The other peaks in the region 1400 – 400 cm^{-1} are the fingerprint of the carbon skeleton.

The purpose of the FTIR analysis is to study in depth the way 4-HBA is attached to the surface of the TiO_2 particles. The TG-DSC measurements (Section 3.1) tend to show that 4-HBA is grafted in the high position via its carboxyl group. FTIR spectra of all samples are presented in Figure 7.

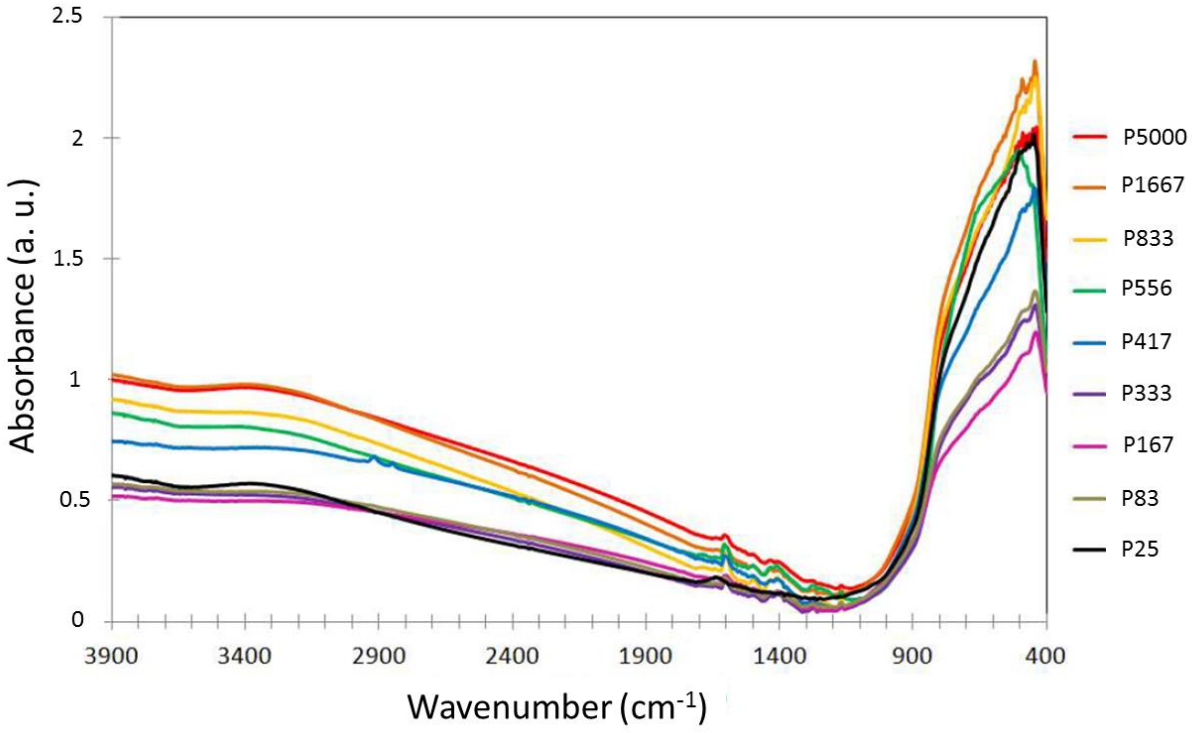

Figure 7: FTIR spectra of all grafted samples.

The functionalized powders and the commercial pristine P25 powder have some identical features: (i) an absorption band around 3400 cm^{-1}, characteristic of the -OH groups of adsorbed water, and (ii) a broad absorption band, under 800 cm^{-1}, related to the characteristic vibrations of TiO_2. However, additional absorption peaks, between 1600 cm^{-1} and 1100 cm^{-1}, are present only for the functionalized powders and not P25. Figure 8 focusses on this specific region.

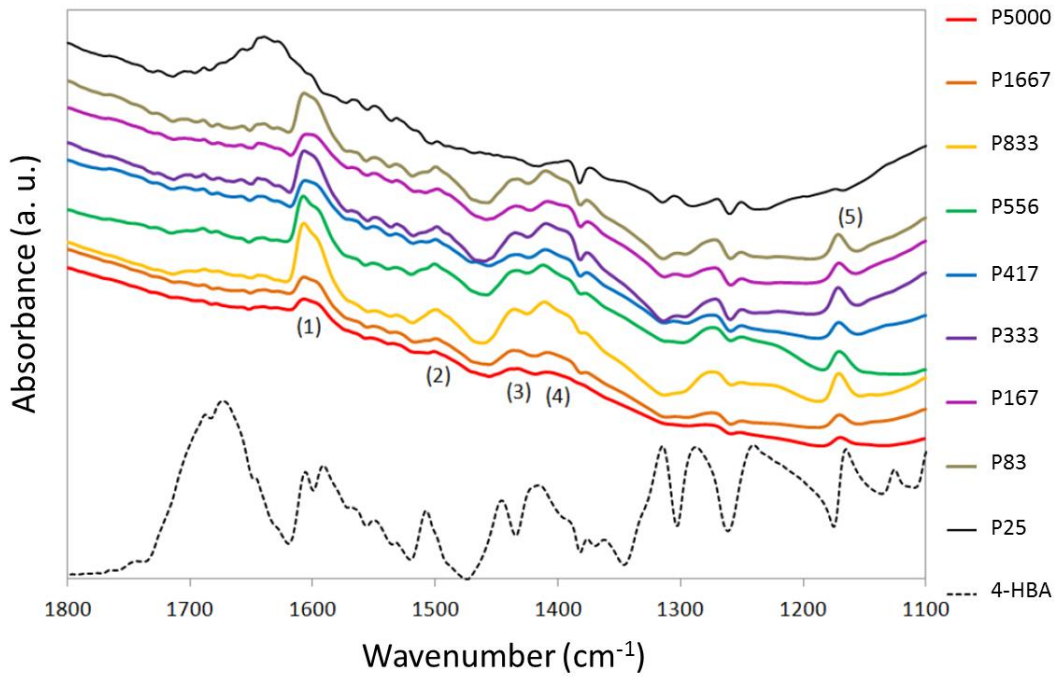

Figure 8: FTIR spectra in the region 1600 cm^{-1} – 1100 cm^{-1} (from Figure 9) in comparison with the 4-HBA spectrum.

Compared to P25, 5 new absorption peaks are observed and numbered in Figure 8. According to the above analysis of FTIR spectrum of 4-HBA, one can determine that the peak (1) is characteristic of the elongation vibration of C - C bonds in the aromatic ring. The peaks (2) and (4) refer, respectively, to asymmetric and symmetric stretching vibrations of the carboxyl groups and the peak (5) corresponds to the vibration due to the bending of the C - OH groups from the alcohol. Therefore, the comparison will highlight some structural changes of the grafted 4-HBA. Peaks (1), (2), (4) and (5) are analyzed in more detail in Table 3, which shows that their positions are close to the vibration wavenumbers initially present in 4-hydroxybenzoic acid. The absorption peak (1) related to the C – C bonds of the benzene ring is still present in all the functionalized powders (Table 3), but slightly shifted. The aromatic cycle is therefore not involved in the functionalization. In addition, the absorption band (5), slightly shifted, attests of the unaltered presence of the hydroxyl groups of the alcohol. The configurations in which the C - OH alcohol group is used for the grafting are therefore eliminated. The

wavenumbers of peaks (1) and (5) are slightly shifted toward higher wavenumbers for grafted samples compared from those of ungrafted 4-HBA molecule, only due to a different environment, mainly the presence of TiO_2.

By opposition, functionalized powders exhibit no absorption peak around 1672 cm^{-1} contrarily to pure 4-HBA spectrum (Figure S3 and dashed line in Figure 8). This means that the C = O double bond in 4-HBA was delocalized during functionalization of TiO_2. Indeed, the acid carboxylic group is deprotonated, shifting the peaks compared to 4-HBA (Table 3). The negative charge of the carboxylate is now delocalized over the entire COO^- function. The only possible surface configurations of the grafted species are then mono- or bi-dentate chelates via the carboxylate group [8].

Table 3: FTIR peak positions

Sample	(1) C - C aromatic (cm^{-1})	(2) asymmetric stretching carboxyl (cm^{-1})	(4) symmetric stretching carboxyl (cm^{-1})	(5) C - OH alcohol bending (cm^{-1})
4-HBA	1591	1508	1416	1165
P5000	1608	1501	1408	1170
P1667	1608	1500	1409	1170
P833	1607	1501	1408	1171
P556	1607	1502	1409	1170
P417	1607	1501	1411	1171
P333	1608	1499	1411	1171
P167	1608	1498	1409	1171
P83	1600	1500	1410	1172

Indeed, the peaks (2) and (4) attest to the presence of the carboxylic group. But, as mentioned above, the shift of peaks (2) from 1508 cm^{-1} around 1500 cm^{-1}, and peaks (4) from 1416 cm^{-1} around 1408 cm^{-1}, is the consequence of the presence of carboxylate $(C(O)O)^-$ groups. These results confirm that the 4-HBA is bound to TiO_2 via a chemical bond through its carboxylic group by formation of mono- or bi-dentate chelates on Ti atoms (see Figure S1 for Scheme of grafted molecule).

3.3. Colloid characterization

In this section, the colloids are analyzed after 3 days at rest. Tables 4 and 5 give the remaining solid percentage after 3 days at rest in ethanol and water respectively.

Table 4: Remaining TiO_2 in suspension after 3 days at rest (in ethanol medium).

[Colloid] / Powder	0.25 g/L (%)	0.5 g/L (%)	1 g/L (%)	3 g/L (%)	5 g/L (%)
P25	7.8	10.6	54	53.6	69.4
P83	0	1.3	5.8	79.4	87.2
P167	0	0	5.3	77.2	87.5
P333	0	0	92.2	94.4	100
P417	0	9.24	70	69.7	75
P556	0	5.3	31.7	80.3	88.6
P833	0	6.6	2	79.8	93.8
P1667	0	0	62.6	81.1	82.1
P5000	0	7.9	1.9	1.5	62.9

Table 5: Remaining TiO_2 in suspension after 3 days at rest (in water medium).

[Colloid] / Powder	0.25 g/L (%)	0.5 g/L (%)	1 g/L (%)	3 g/L (%)	5 g/L (%)
P25	15.5	0	0	62.7	70.3
P83	10.5	4	0	86.7	88.8
P167	60.8	6.5	1.9	91.9	92.9
P333	16	1.3	94.4	99.5	94.6
P417	0	45.8	78.3	84.4	84.4
P556	100	11.9	89.2	96.2	100
P833	100	0	92.6	92.2	94.5
P1667	0	2.6	92.2	91.3	95.1
P5000	68.51	47.8	0	93	89.3

General trends emerge from Tables 4 and 5. First, from Table 4, it is observed that the colloids prepared at 0.25 and 0.5 g/L are globally not stable as all the solid has precipitated. But from 1 g/L, it seems that colloids in ethanol are more and more stable when the concentration of powder increases. In Table 5, at the concentration of 0.25 g/L and 0.5 g/L, it is difficult to interpret the

results in water medium. But from a concentration of powder equal to 1 g/L, colloids in water are more stable than to those made in ethanol.

Finally, the functionalized powder giving the most stable colloids at the three highest concentrations (1g/L, 3 g/L and 5 g/L) is the P333 sample, independently of the solvent. With this powder, around 75% of the surface is covered with 4-HBA (Table 2). This sample is chosen for the photocatalytic experiments and its photoactivity is compared to pure P25.

In Table 6, the zeta potential value is higher for P333 sample than P25 and the hydrodynamic diameter is smaller for P333 sample. This information confirms that P333 sample produces more stable colloids in water than P25. Indeed, the higher the zeta potential is, the more stable the suspension is. Moreover, smaller aggregates (lower d_{DLS}) lead to more stable suspensions.

Table 6: Stability data for the water colloids of P333 and P25 samples.

Sample	Zeta potential (mV)	d_{DLS} (nm)
P333	19.3	163
P25	3.6	715

3.4. Further characterizations of the P333 sample compared to P25

TEM pictures of P25 and P333 samples are depicted in Figure 9. For both samples, TiO_2 particles with size around 20-30 nm can be observed with no difference between the samples. Indeed, the grafted 4-HBA molecules are not visible with this TEM device. The grafting has no influence on the morphology and size of the TiO_2 particles.

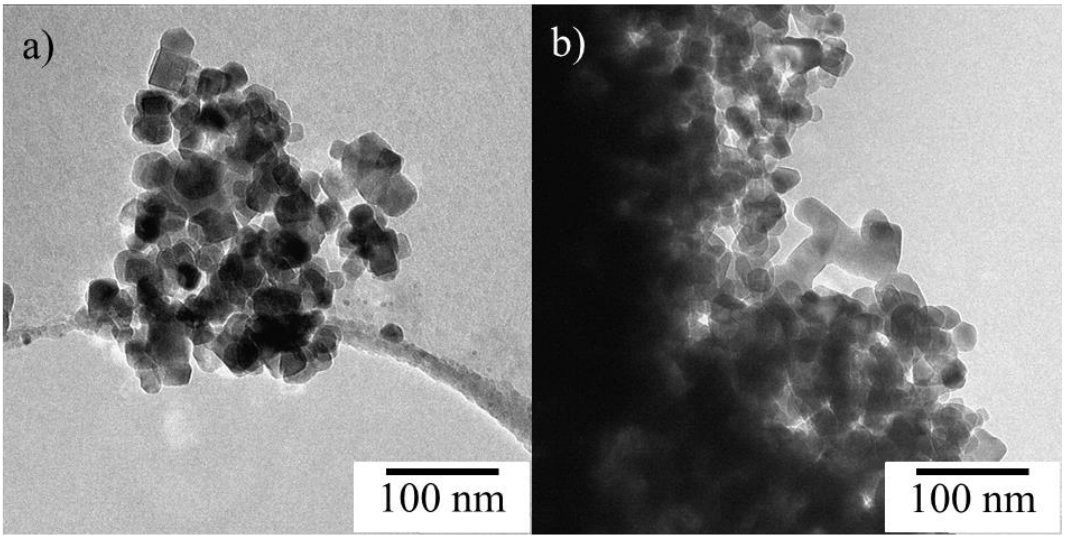

Figure 9: TEM pictures of (a) P25 and (b) P333 samples.

Ti *2p*, O *1s*, N *1s*, and C *1s* XPS spectra are presented in Figure 10 for P25 (blue curves) and P333 (orange curves) samples. Both samples present similar XPS spectra. The quantification, peak position and full width at half maximum (FWHM) are presented in Table 7.

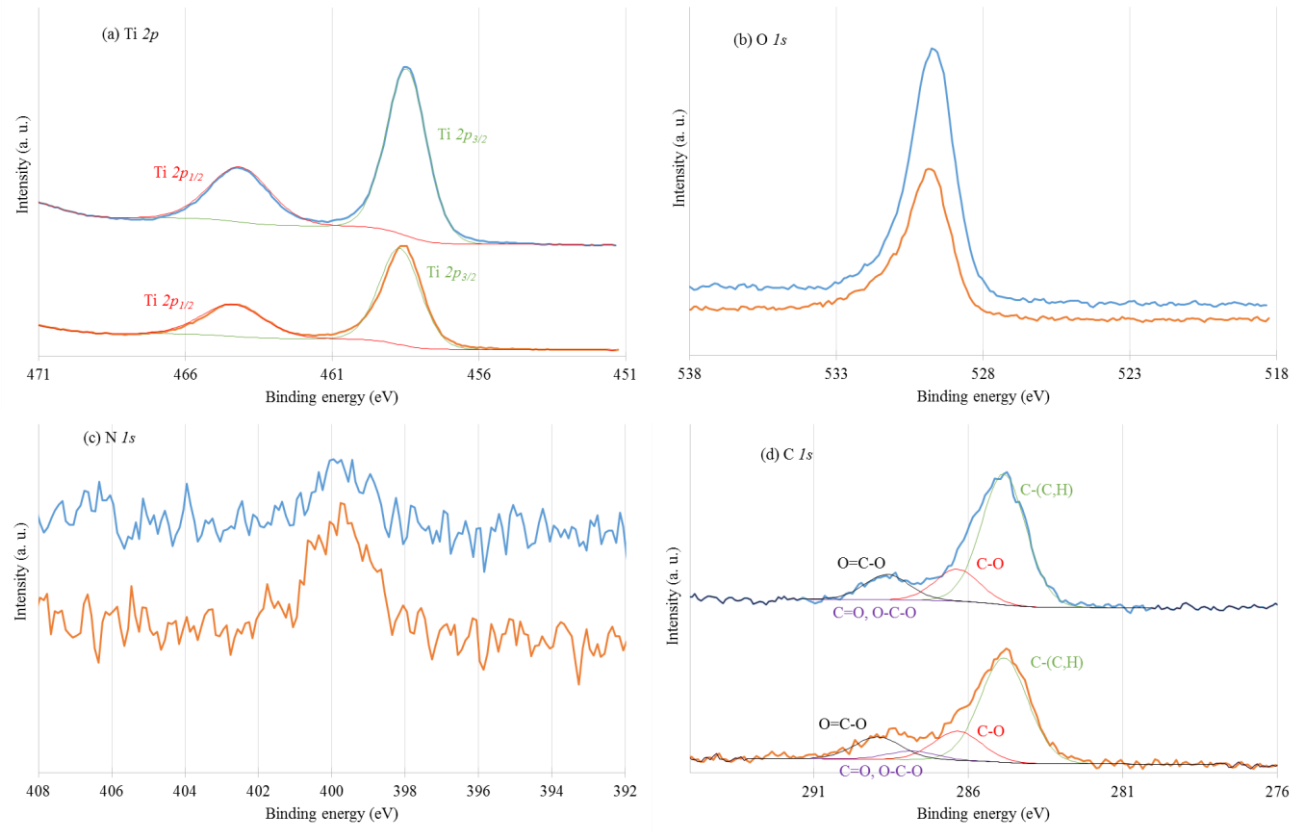

Figure 10: XPS spectra of P25 (blue) and P333 (orange) samples: (a) Ti *2p* region, (b) O *1s* region, (c) N *1s* region and (d) C *1s* region.

On the Ti *2p* spectra (Figure 10a), for both samples, the Ti $2p_{1/2}$ and Ti $2p_{3/2}$ peaks are observed at (464.1-464.3) eV and (458.5-458.6) eV respectively. They are attributed to Ti^{4+} species [42–44] and therefore the expected TiO_2 [36].

For the O *1s* spectra (Figure 10b), both samples present a peak at (529.8-529.9) eV corresponding to Ti-O bonds in TiO_2 [36,45]. The shoulder at higher binding energy in the O *1s* peak is hardly exploitable because of the presence of a non-negligible amount of oxygen involved in the common carbonaceous contamination (Figure 10d) [36].

For the N *1s* spectra (Figure 10c), one peak is observed around (399.7-399.8) eV with a quantification of 0.4 at.%. According to literature, a N *1s* peak around 400 eV may correspond to interstitial Ti-O-N bonds [46,47].

For the C *1s* region (Figure 10d), the signal can be decomposed in three/four different peaks depending on the sample: (i) one at 284.8 eV corresponding to C-(C,H) bonds, (ii) another at (286.3-286.4) eV corresponding to C-O bonds, (iii) a peak around 287.8 eV corresponding to C=O or O-C-O bonds (only for P333 sample) and (iv) a fourth at (288.6-288.8) eV corresponding to O=C-O bonds.

The quantification, presented in the Table 7, highlights some differences between the two samples. Especially the amount of carbon is higher for P333 sample, which is consistent with the presence of 4-HBA molecules. Indeed, the amount of O=C-O and C-O groups are higher with P333 sample as 4-HBA molecule contains these groups. The presence of 4-HBA molecules at the surface of P333 sample is attested.

Table 7: XPS atomic quantification, peak positions and FWHM for P25 and P333 samples.

	P25	P333

	Atomic concentration (at%)	Peak position (eV)	FWHM	Atomic concentration (at%)	Peak position (eV)	FWHM
O=C-O	1.68	288.6	1.7	2.52	288.8	1.8
C=O, O-C-O	0	287.9	1.7	0.98	287.8	1.8
C-O	2.12	286.4	1.7	3.30	286.3	1.8
C-(C,H)	8.64	284.8	1.7	11.78	284.8	1.8
C *1s* total	**12.43**	-	-	**18.59**	-	-
Ti $2p_{2/3}$	14.13	458.5	1.6	13.29	458.6	1.6
Ti $2p_{1/2}$	7.09	464.1	2.5	6.67	464.3	2.5
Ti *2p* total	**21.23**	-	-	**19.96**	-	-
N *1s* total	**0.29**	**399.7**	**1.9**	**0.75**	**399.8**	**2.1**
O *1s* total	**66.05**	**529.8**	**1.7**	**60.71**	**529.9**	**1.9**
O bonded to C	5.47	-	-	8.34	-	-
O remaining	60.58	-	-	52.37	-	-
O remaining/Ti	2.85	-	-	2.62	-	-

The normalized Kubelka-Munk function is presented in Figure 11 for P25 and P333 samples. A shift towards higher wavelength is observed for P333 sample compared to P25 sample. It was previously shown in [20,21,23] that the grafting of molecules such as 4-HBA can produce a red shift of the absorption spectrum. This allows electron transfer from the grafted molecule to the TiO_2 leading to enhance photoactivity in visible range.

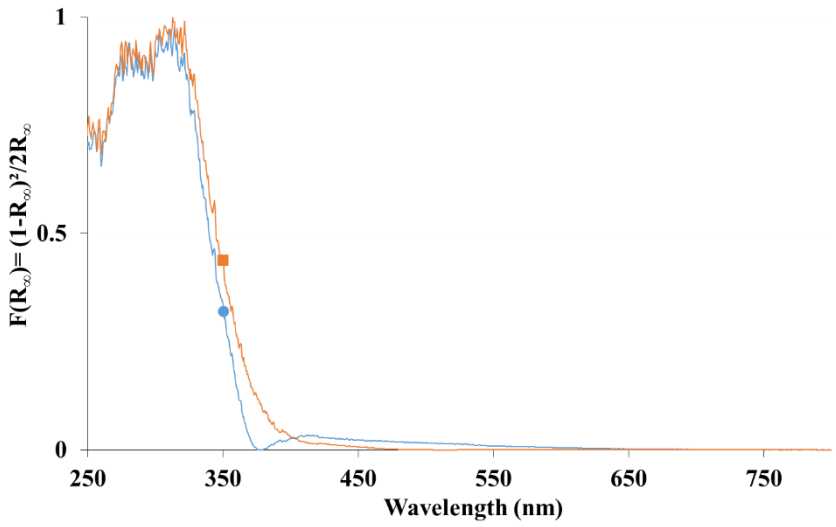

Figure 11: Normalized Kubelka-Munk function F(R∞) calculated from DRUV-Vis spectra for samples: (●) P25, and (■) P333.

3.5.Photocatalytic activity

The photoactivity of P25 and P333 is assessed on the PNP degradation with a concentration of 0.25 or 1 g/L without or with stirring. The results are presented in Figure 12. Without stirring during the catalytic test (Figure 12a), the PNP degradation is lower with P25 than P333. The difference is more pronounced with the concentration of 0.25 g/L, 7% vs. 56% for P25 and P333 respectively. The results are consistent with the study of the colloid stability (Section 3.3) where the positive effect of 4-HBA on the colloid stability is pointed out. So, during illumination, the stable colloid (P333) will have a large amount of TiO_2 activated by the light and a large surface in contact with solution and therefore with PNP. As catalysis is a surface effect, this allows a high degradation activity. On the contrary, when only P25 is used, the powder precipitates in the flask, and only a very small portion of the TiO_2 is illuminated, reducing its photocatalytic activity.

With stirring (Figure 12b), the activity increases with both catalysts at the two concentrations. The P333 catalyst remains slightly better than P25 sample even if the difference is smaller. This improvement with P333 can be due to the 4-HBA molecules which can enhance the photoactivity due to electron transfer form 4-HBA to TiO_2 [23]. Nevertheless, the better activity obtained for P333 without stirring proves the efficiency of the grafting on the dispersion of TiO_2 particles and the stability of the colloids produced. A good dispersion is beneficial to a higher photoactivity.

The difference in activity between the two concentrations could be explained by the difference in turbidity of the suspensions (Figure S4). Indeed, a less turbid suspension (concentration at 0.25 g/L) allows a better light penetration during the photocatalytic experiment.

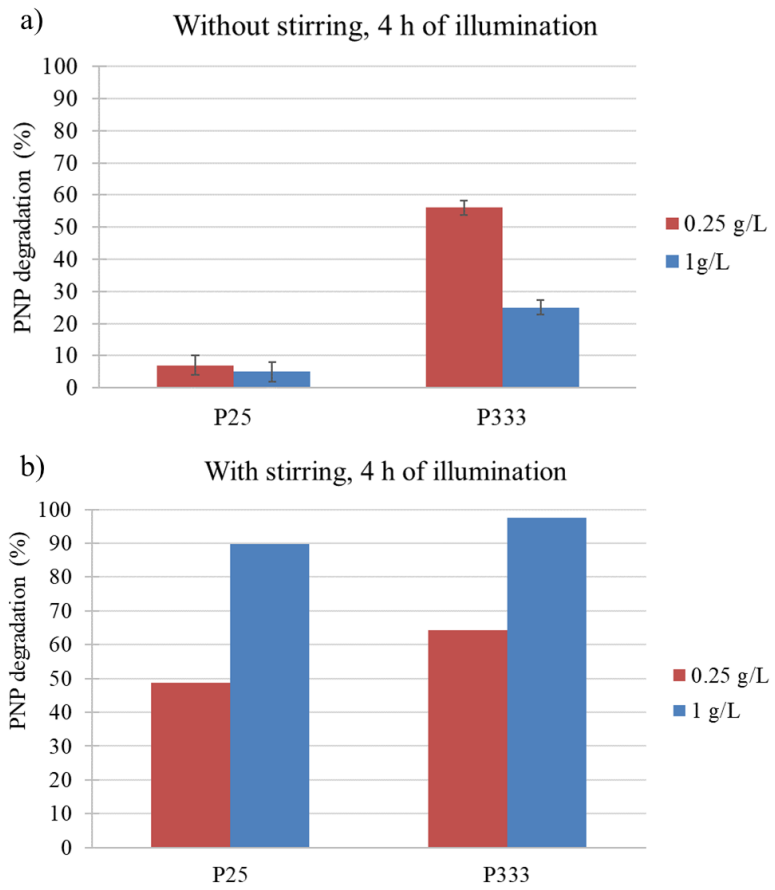

Figure 12: Photocatalytic degradation of PNP after 4 h of illumination (a) without and (b) with stirring for a catalyst concentration of 0.25 and 1 g/L.

To assess the stability of the 4-HBA grafting to P25, recycling experiments (catalyst concentration of 0.25 g/L without stirring) are performed with the P333 and P25 samples. In Figure 13, the results of six consecutive photoactivity tests on PNP degradation are presented for both samples. The degradation activity remains constant during the experiments, the P333 sample keeping a better activity than the P25 sample. It tends to show that the grafting stays stable during the 24 h of illumination, the hypothesis of a covalent bonding between titania surface and the organic molecule through C-O-Ti bonds being reinforced.

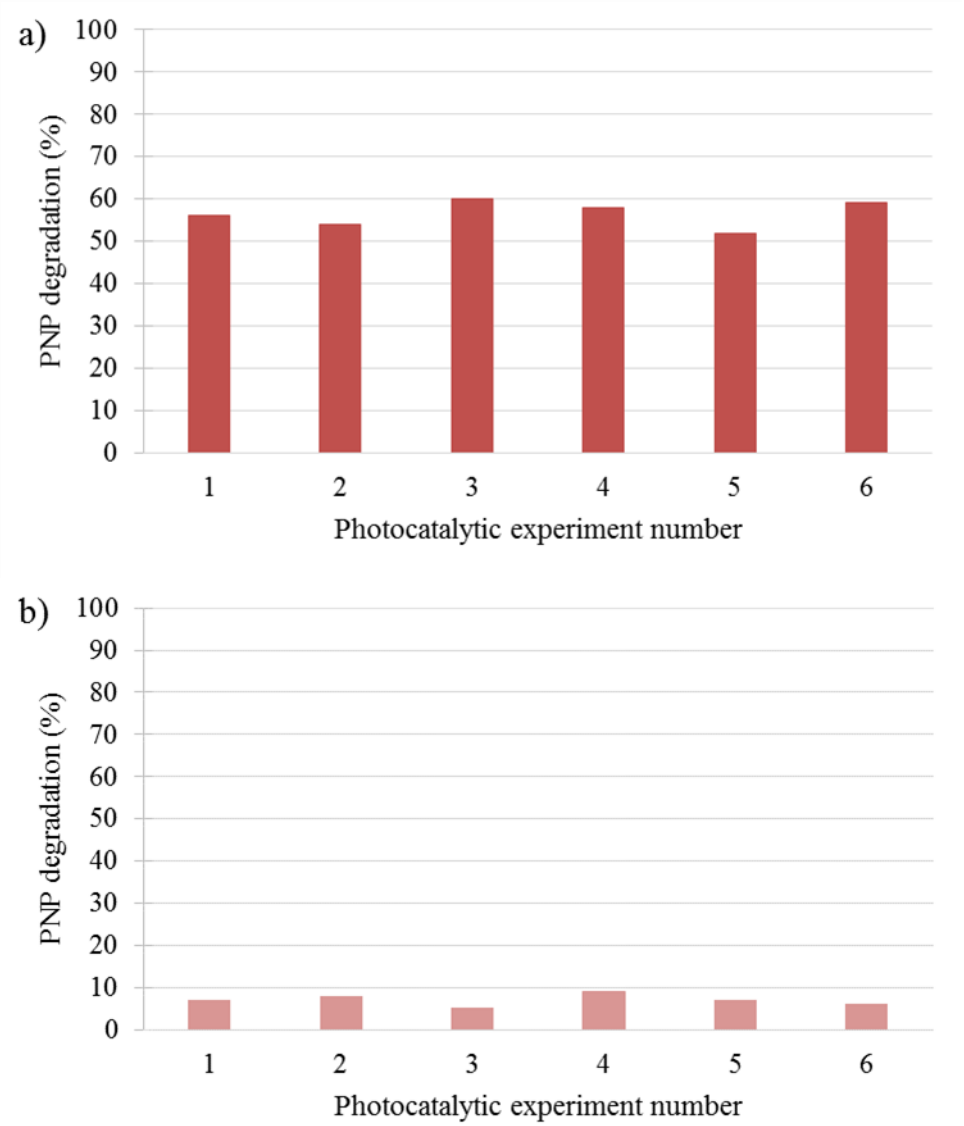

Figure 13: Recycling photocatalytic degradation of PNP with 6 x 4 h of illumination with (a) P333 and (b) P25 without stirring for a catalyst concentration of 0.25 g/L.

4. Conclusions

In this work, 4-hydroxybenzoic acid was grafted on TiO_2 Evonik Aeroxide P25 powder in order to produce stable colloids. The pure Evonik Aeroxide P25 was used as reference material. Different amounts of 4-HBA were grafted on P25.

Results showed that 4-HBA is grafted by its carboxylic group on the P25 surface. The ratio between P25 and 4-HBA is an important parameter which influences the adsorption of the 4-HBA. Indeed, if the amount of 4-HBA is too high compared to the TiO_2 available surface, the interactions between 4-HBA molecules are favored, reducing the adsorption on P25.

The grafting of 4-HBA on P25 produced stable colloids in both ethanol and water medium. The optimized sample, with 4-HBA/TiO_2 mass ratio of 0.333, showed the highest stability in both media. This sample was further tested and compared to P25 for the PNP degradation under UV-visible light. These photocatalytic experiments without stirring highlight the beneficial effect of the powder stability.The grafted sample reached higher degradation percentages (up to 8 times) than pure Evonik Aeroxide P25.

This functionalization method is easy to implement and stabilizes colloids starting from pre-synthesized powders. This opens the door for further developments such as in coating field.

Acknowledgements

S.D.L., S.H. and N.B. are grateful to F.R.S.-F.N.R.S for their Senior Research Associate, Research Director positions and FRIA grant respectively. The authors acknowledge the Ministère de la Région Wallonne Direction Générale des Technologies, de la Recherche et de l'Energie (DGO6), the Fonds de Bay, the Fonds de Recherche Fondamentale et Collective and Innoviris Brussels for financial supports.

This paper is dedicated to Carlos Alberto Pàez, the director of this work, who passed away the 12th July 2020.

Compliance with ethical standards

Conflict of interest: The authors declare that they have no conflicts of interest.

Data availability

The raw/processed data required to reproduce these findings cannot be shared at this time as the data also forms part of an ongoing study.

References

[1] M. Iijima, M. Kobayakawa, H. Kamiya, Tuning the stability of TiO2 nanoparticles in various solvents by mixed silane alkoxides, J. Colloid Interface Sci. 337 (2009) 61–65. doi:10.1016/j.jcis.2009.05.007.

[2] J.G. Mahy, V. Claude, L. Sacco, S.D. Lambert, Ethylene polymerization and hydrodechlorination of 1,2-dichloroethane mediated by nickel (II) covalently anchored to silica xerogels, J. Sol-Gel Sci. Technol. 81 (2017) 59–68. doi:10.1007/s10971-016-4272-0.

[3] G.L.-M. Léonard, C.A. Pàez, A.E. Ramírez, J.G. Mahy, B. Heinrichs, Interactions between Zn2+ or ZnO with TiO2 to produce an efficient photocatalytic, superhydrophilic and aesthetic glass, J. Photochem. Photobiol. A Chem. 350 (2018). doi:10.1016/j.jphotochem.2017.09.036.

[4] K. Guan, Relationship between photocatalytic activity, hydrophilicity and self-cleaning effect of TiO2/SiO2 films, Surf. Coatings Technol. 191 (2005) 155–160. doi:10.1016/j.surfcoat.2004.02.022.

[5] G.L.-M. Léonard, C.M. Malengreaux, Q. Mélotte, S.D. Lambert, E. Bruneel, I. Van Driessche, et al., Doped sol–gel films vs. powders TiO2: On the positive effect induced by the presence of a substrate, J. Environ. Chem. Eng. 4 (2016) 449–459. doi:10.1016/j.jece.2015.11.040.

[6] Y. Wang, Z. Huang, R.S. Gurney, D. Liu, Superhydrophobic and photocatalytic PDMS/TiO2 coatings with environmental stability and multifunctionality, Colloids Surfaces A Physicochem. Eng. Asp. 561 (2019) 101–108. doi:10.1016/j.colsurfa.2018.10.054.

[7] M. Houmard, D. Riassetto, F. Roussel, A. Bourgeois, G. Berthomé, J.C. Joud, et al., Morphology and natural wettability properties of sol-gel derived TiO2-SiO2 composite thin films, Appl. Surf. Sci. 254 (2007) 1405–1414. doi:10.1016/j.apsusc.2007.06.072.

[8] K. Wu, Y. Wang, I. Zhitomirsky, Electrophoretic deposition of TiO2 and composite TiO2-MnO2 films using benzoic acid and phenolic molecules as charging additives, J. Colloid Interface Sci. 352 (2010) 371–378. doi:10.1016/j.jcis.2010.08.059.

[9] D. Cambié, C. Bottecchia, N.J.W. Straathof, V. Hessel, T. Noël, Applications of Continuous-Flow Photochemistry in Organic Synthesis, Material Science, and Water Treatment, Chem. Rev. 116 (2016) 10276–10341. doi:10.1021/acs.chemrev.5b00707.

[10] N. Emmanuel, C. Mendoza, M. Winter, C.R. Horn, A. Vizza, L. Dreesen, et al., Scalable Photocatalytic Oxidation of Methionine under Continuous-Flow Conditions, Org. Process Res. Dev. 21 (2017) 1435–1438. doi:10.1021/acs.oprd.7b00212.

[11] O.O. Van der Biest, L.J. Vandeperre, Electrophoretic deposition of Materials, Annu. Rev. Mater. Sci. 29 (1999) 327–352. http://www.substech.com/dokuwiki/doku.php?id=electrophoretic_deposition.

[12] A. Kohut, S. Ranjan, A. Voronov, W. Peukert, V. Tokarev, O. Bednarska, et al., Design of a new invertible polymer coating on a solid surface and its effect on dispersion colloidal stability, Langmuir. 22 (2006) 6498–6506. doi:10.1021/la060162u.

[13] I. Zhitomirsky, A. Petric, Electrophoretic deposition of YSZ powders for solid oxide

fuel cells, J. Mater. Sci. 39 (2004) 825–831.

[14] B. Ferrari, S. Gonzalez, R. Moreno, C. Baudin, Multilayer coatings with improved reliability produced by aqueous electrophoretic deposition, J. Eur. Ceram. Soc. 26 (2006) 27–36. doi:10.1016/j.jeurceramsoc.2004.10.018.

[15] M. Feng, C. Gu, C. Bao, X. Chen, H. Yan, Z. Shi, et al., Synthesis of a benzyl-grafted alginate derivative and its effect on the colloidal stability of nanosized titanium dioxide aqueous suspensions for Pickering emulsions, RSC Adv. (2018) 34397–34407. doi:2018/RA/C8RA04300K.

[16] J.S. Gebauer, V. Mackert, S. Ognjanović, M. Winterer, Tailoring metal oxide nanoparticle dispersions for inkjet printing, J. Colloid Interface Sci. 526 (2018) 400–409. doi:10.1016/j.jcis.2018.05.006.

[17] Q. Zhang, I. Lee, J.I.B. Joo, F. Zaera, Y. Yin, Core-Shell Nanostructured Catalysts, Acc. Chem. Res. 46 (2013) 1816–1824.

[18] B. Peng, Y. Liu, G.A.L. Aarts, R.P.A. Dullens, Stabilisation of hollow colloidal TiO2 particles by partial coating with evenly distributed lobes, Soft Matter. 17 (2021) 1447–1702. doi:10.1039/d0sm02100h.

[19] P.A. Connor, K.D. Dobson, A.J. McQuillan, New Sol-Gel Attenuated Total Reflection Infrared Spectroscopic Method for Analysis of Adsorption at Metal Oxide Surfaces in Aqueous Solutions. Chelation of TiO2, ZrO2, and Al2O3 Surfaces by Catechol, 8-Quinolinol, and Acetylacetone, Langmuir. 11 (1995) 4193–4195. doi:10.1021/la00011a003.

[20] G.L. Wang, J.J. Xu, H.Y. Chen, Dopamine sensitized nanoporous TiO2film on electrodes: Photoelectrochemical sensing of NADH under visible irradiation, Biosens.

Bioelectron. 24 (2009) 2494–2498. doi:10.1016/j.bios.2008.12.031.

[21] T.D. Savić, M.I. Ćomor, N.D. Abazović, Z. V. Šaponjić, M.T. Marinović-Cincović, D. Veljković, et al., Anatase nanoparticles surface modified with fused ring salicylate-type ligands (1-hydroxy-2-naphthoic acids): A combined DFT and experimental study, J. Alloys Compd. 630 (2015) 226–235. doi:10.1016/j.jallcom.2015.01.041.

[22] T.D. Savić, I.A. Janković, Z. V Šaponjić, M.I. Čomor, D.Ž. Veljković, S.D. Zarić, et al., Surface modification of anatase nanoparticles with fused ring catecholate type ligands: a combined DFT and experimental study of optical properties, Nanoscale. 4 (2012) 1612–1619. doi:10.1039/C2NR11501H.

[23] J. Moser, S. Punchihewa, P.P. Infelta, M. Grätzel, Surface Complexation of Colloidal Semiconductors Strongly Enhances Interfacial Electron-Transfer Rates, Langmuir. 7 (1991) 3012–3018. doi:10.1021/la00060a018.

[24] H. Frei, D.J. Fitzmaurice, M. Grätzel, Surface Chelation of Semiconductors and Interfacial Electron Transfer, Langmuir. 6 (1990) 198–206. doi:10.1021/la00091a032.

[25] B. Chu, 7 Dynamic Light Scattering, (2008).

[26] P. Kubelka, New contributions to the optics of intensely light-scattering materials., J. Opt. Soc. Am. 38 (1948) 448–457. doi:10.1364/JOSA.44.000330.

[27] C.M. Malengreaux, S. Douven, D. Poelman, B. Heinrichs, J.R. Bartlett, An ambient temperature aqueous sol–gel processing of efficient nanocrystalline doped TiO2-based photocatalysts for the degradation of organic pollutants, J. Sol-Gel Sci. Technol. 71 (2014) 557–570. doi:10.1007/s10971-014-3405-6.

[28] J.G. Mahy, S.D. Lambert, G.L.M. Léonard, A. Zubiaur, P.Y. Olu, A. Mahmoud, et al., Towards a large scale aqueous sol-gel synthesis of doped TiO2: Study of various

metallic dopings for the photocatalytic degradation of p-nitrophenol, J. Photochem. Photobiol. A Chem. 329 (2016) 189–202. doi:10.1016/j.jphotochem.2016.06.029.

[29] J.G. Mahy, V. Cerfontaine, D. Poelman, F. Devred, E.M. Gaigneaux, B. Heinrichs, et al., Highly efficient low-temperature N-doped TiO2 catalysts for visible light photocatalytic applications, Materials (Basel). 11 (2018) 1–20. doi:10.3390/ma11040584.

[30] J.G. Mahy, S.D. Lambert, G.L.-M. Léonard, A. Zubiaur, P.-Y. Olu, A. Mahmoud, et al., Towards a large scale aqueous sol-gel synthesis of doped TiO2: Study of various metallic dopings for the photocatalytic degradation of p-nitrophenol, J. Photochem. Photobiol. A Chem. 329 (2016) 189–202. doi:10.1016/j.jphotochem.2016.06.029.

[31] C.A. Páez, D.Y. Liquet, C. Calberg, S.D. Lambert, I. Willems, A. Germeau, et al., Study of photocatalytic decomposition of hydrogen peroxide over ramsdellite-MnO2 by O2-pressure monitoring, Catal. Commun. 15 (2011) 132–136. doi:10.1016/j.catcom.2011.08.025.

[32] J.G. Mahy, G.L.-M. Léonard, S. Pirard, D. Wicky, A. Daniel, C. Archambeau, et al., Aqueous sol-gel synthesis and film deposition methods for the large-scale manufacture of coated steel with self-cleaning properties, J. Sol-Gel Sci. Technol. 81 (2017) 27–35. doi:10.1007/s10971-016-4020-5.

[33] C.H. Giles, A.P. D'Silva, I.A. Easton, A general treatment and classification of the solute adsorption isotherm part. II. Experimental interpretation, J. Colloid Interface Sci. 47 (1974) 766–778. doi:10.1016/0021-9797(74)90253-7.

[34] C.H. Giles, D. Smith, A. Huitson, A General Treatment and Classification of the Solute Adsorption Isotherm part I Theoretical, J. Colloid Interface Sci. 47 (1974) 755–765.

[35] C.H. Giles, H. V Mehta, C.E. Stewart, R.V.R. Subramanian, Adsorption at lnorganic Surfaces. Part I. An Investigation into the Mechanism of Adsorption of Organic Compounds by the Anodic Film on Aluminium, J. Chem. Soc. (1954) 4360–4374.

[36] J.G. Mahy, S.D. Lambert, R.G. Tilkin, D. Poelman, C. Wolfs, F. Devred, et al., Ambient temperature ZrO2-doped TiO2 crystalline photocatalysts : Highly efficient powders and films for water depollution, Mater. Today Energy. 13 (2019) 312–322. doi:10.1016/j.mtener.2019.06.010.

[37] W. Emmanuel, G. Fabien, M. Christophe, Thermogravimétrie, Tech. l'ingénieur Méthodes Therm. d'analyse. base docum (2014). https://www.techniques-ingenieur.fr/base-documentaire/mesures-analyses-th1/methodes-thermiques-d-analyse-42384210/thermogravimetrie-p1260/.

[38] K. Nazeeruddin, M. Amirnasr, P. Comte, J.R. Mackay, A.J. McQuillan, R. Houriet, et al., Adsorption studies of counterions carried by the sensitizer cis-dithiocyanato(2,2′-bipyridyl-4,4′-dicarboxylate) ruthenium(II) on nanocrystalline TiO2 films, Langmuir. 16 (2000) 8525–8528. doi:10.1021/la000685g.

[39] M. Amirnasr, M.K. Nazeeruddin, M. Grätzel, Thermal stability of cis-dithiocyanato(2,2′-bipyridyl4,4′dicarboxylate) ruthenium(II) photosensitizer in the free form and on nanocrystalline TiO2films, Thermochim. Acta. 348 (2000) 105–114.

[40] L. Shi, Q. Liu, X. Guo, W. He, Z. Liu, Pyrolysis of coal in TGA: Extent of volatile condensation in crucible, Fuel Process. Technol. 121 (2014) 91–95. doi:10.1016/j.fuproc.2014.01.013.

[41] X.G. Li, Y. Lv, B.G. Ma, W.Q. Wang, S.W. Jian, Decomposition kinetic characteristics of calcium carbonate containing organic acids by TGA, Arab. J. Chem. 10 (2017) S2534–S2538. doi:10.1016/j.arabjc.2013.09.026.

[42] J.G. Mahy, V. Cerfontaine, D. Poelman, F. Devred, E.M. Gaigneaux, B. Heinrichs, et al., Highly efficient low-temperature N-doped TiO2 catalysts for visible light photocatalytic applications, Materials (Basel). 11 (2018). doi:10.3390/ma11040584.

[43] K. Maver, U.L. Štangar, U. Černigoj, S. Gross, R. Cerc Korošec, Low-temperature synthesis and characterization of TiO2 and TiO2-ZrO2 photocatalytically active thin films, Photochem. Photobiol. Sci. 8 (2009) 657–662. doi:10.1039/b817475j.

[44] T.V.L. Thejaswini, D. Prabhakaran, M.A. Maheswari, Synthesis of mesoporous worm-like ZrO2–TiO2 monoliths and their photocatalytic applications towards organic dye degradation, J. Photochem. Photobiol. A Chem. 344 (2017) 212–222. doi:10.1016/j.jphotochem.2017.05.015.

[45] M. Li, X. Li, G. Jiang, G. He, Hierarchically macro – mesoporous ZrO 2 – TiO 2 composites with enhanced photocatalytic activity, Ceram. Int. 41 (2015) 5749–5757. doi:10.1016/j.ceramint.2014.12.161.

[46] R. Azouani, S. Tieng, K. Chhor, J.F. Bocquet, P. Eloy, E.M. Gaigneaux, et al., TiO2 doping by hydroxyurea at the nucleation stage: towards a new photocatalyst in the visible spectral range, Phys. Chem. Chem. Phys. 12 (2010) 1–10.

[47] C. Bittencourt, M. Rutar, P. Umek, A. Mrzel, K. Vozel, D. Arcon, et al., Molecular nitrogen in N-doped TiO2 nanoribbons, RSC Adv. 5 (2015) 23350–23356. doi:10.1039/C4RA14410D.